# Discussion of assumptions behind rule-based ice loads due to crushing

Ekaterina Kim[*, a, b] & Jørgen Amdahl [a, b]

[a]Centre for Autonomous Marine Operations and Systems (AMOS), Norwegian University of Science and Technology, 7491 Trondheim, Norway

[b]Centre for Sustainable Arctic Marine and Coastal Technology (SAMCoT), Norwegian University of Science and Technology, 7491 Trondheim, Norway

*Abstract*

Forecasts and trends indicate an increase in marine operations in polar waters. The design of new ships for severe polar conditions is usually solved via theoretical considerations that are combined with previous experience and engineering judgment. A deeper understanding of the theoretical considerations that underlie rule-based formulations is required for designing safe and efficient structures. This paper focuses on the assumptions that are hidden in the ice load formulations of the International Association of Classification Societies (IACS) Unified Requirements for Polar Ships (IACS 2011) and of the Russian Maritime Register of Shipping (RMRS) Rules for the Classification and Construction of Sea-going Ships (RMRS 2014), particularly the Daley ice load model and the Kurdyumov and Kheisin hydrodynamic model for ice crushing. A qualitative comparison of the two models is presented. The assumptions that underlie rule-based ice loads in the bow area are placed in the context of current understanding of ice-structure interaction process. The comparison of the models demonstrates that the underlying assumptions regarding the pressure-area relationship, ice edge spalling characteristics, dynamic viscosity and strength of the crushed ice are the most important assumptions, although they are highly contentious.

[*]Corresponding author. Tel.: +47 735 95710. E-mail addresses: ekaterina.kim@ntnu.no (E. Kim), jorgen.amdahl@ntnu.no (J. Amdahl)

## 1. *Introduction*

Marine operations and maritime transportation are extending into polar waters. The ice loads on fixed and floating structures are not fully understood, but empirical estimates are abundant in existing offshore standards and ship rules. In the context of ice loads, accumulated experience and engineering judgment have become essential components of the design process. Engineers are often faced with situations in which the adequate experience does not exist. Hence, to design safe and robust structures, a deeper understanding of the scientific basis for rule-based ice load formulations is required. To achieve this goal, there is a need to clarify the basis of the rule formulations. For example, Russia is considered to be the most experienced nation with respect to ship operations in polar waters (Barents 2020, 2009). However, the scientific basis for ice load formulations of the Russian Maritime Register of Shipping (RMRS) Rules for the Classification and Construction of Sea-going Ships (RMRS 2014) is difficult to find, and it is often criticized outside of Russia; refer the discussion on design ice pressures in Riska (2011). The International Association of Classification Societies (IACS) Unified Requirements for Polar Ships have been gradually accepted by the industry as a design standard for vessels that operate in polar waters. However, only a few people are aware of the assumptions behind rationale of IACS ice loads.

This paper discusses the ice load models that were used to determine the IACS and RMRS rules, which are the *Daley model* for an oblique collision with a floating ice edge and the *Kurdyumov and Kheisin hydrodynamic model* (HDM) of ice crushing during a hull-ice contact. In the context of current understanding of ice-structure interaction process, a qualitative comparison of these models is presented.

This paper does not address the background of the important Finnish-Swedish Ice Class Rules (FSICR), and the discussions refer only to deterministic design formulations. Riska and

Kämäräinen (2011) performed a comprehensive overview of the principles that underlie the FSICR. A probabilistic approach to design was presented by Kaldasaun and Kujala (2011) for ships that navigate in the Baltic Sea and by Ralph and Jordaan (2013) for Arctic ships; interested readers are referred to those papers for details.

## *2. Background*

A system of equations is used to determine the actual scantling requirements (e.g., plating and frames) for different ice loads. Table 1 presents a comparison of the IACS and RMRS ice loads and requirements for transversely framed shell plating.

Table 1. Rule formulae of the IACS Unified Requirements and the RMRS Rules.

| Rule | IACS (Sec. I2.3) | RMRS (Vol. 1 Pt. 2 Sec. 3.10.3.2) |
|---|---|---|
| Ice pressure in the bow sub-region | $p[MPa] = fa^{0.22} \cdot CF_c^{0.22} \cdot CF_D^{2} \cdot AR^{0.3} \cdot M^{0.14}$ | $p[\mathrm{kPa}] = 2500 \cdot a_1 \cdot v_m \cdot M^{0.17}$ |
| Load patch height (m) | $b = fa^{0.39} \cdot CF_c^{0.39} \cdot CF_D^{-1} \cdot AR^{-0.65} \cdot M^{0.25}$ | $b = C_1 \cdot u_m \cdot M^{0.33}$ |
| Requirement of shell plating thickness (mm) | $t[\mathrm{mm}] = 500s\sqrt{\frac{PPF \cdot p[\mathrm{MPa}]}{\sigma_y}} \cdot \frac{1}{1+0.5\frac{s}{b}} + t_s$<br><br>$t_s$ is the corrosion and abrasion allowance; $t_s$ is in the range of 2.0 – 7.0 mm depending on three factors: hull area, ice class and the presence/absence of an effective coating system. | $t[\mathrm{mm}] = 15.8s\sqrt{\frac{p[\mathrm{kPa}]}{\sigma_y}} \cdot \frac{1}{1+0.5\frac{s}{b}} + t_s$<br><br>$t_s$ is the corrosion and abrasion allowance; $t_s$=0.75$T \cdot u$, where $T$ is the planned ship life, in years; $u$ is the annual reduction of shell plating thickness as a |

| | | |
|---|---|---|
| | | result of corrosion, wear and abrasion; $u$ depends on the hull region and ice class and is in the range of 0.2 – 0.7 mm/year. |

$M$ is the vessel displacement (kilotons); $\sigma_y$ is the yield stress of the material (MPa) which is determined in accordance with the IACS and RMRS rules; $s$ is the frame spacing (m). *In the RMRS formulae*, $a_1$ and $C_1$ are ice class factors in the ranges of 0.36−7.9 and 0.38−0.64, respectively, and $v_m$ and $u_m$ are hull shape factors, which depend on the location of the sub-region considered and the hull configuration parameters in this sub-region. *In the IACS rules*, $CD_c$ and $CF_D$ are ice class factors, i.e., $CD_c$ = (1.80−17.69) is the crushing failure factor and $CF_D$ = (1.11–2.01) is the load patch dimensions factor; $PPF$ is the pressure peak factor, where $PPF = (1.8–s) \geq 1.2$; $AR$ is the load patch aspect ratio; $fa$ is the hull shape factor ($fa \leq 0.6$), which accounts for the bending failure of ice and depends on ice properties, the location of the sub-region and the hull angles in the sub-region.

Table 1 indicates that the plate thickness requirements in both the IACS and RMRS rules are based on the plastic bending behavior of the plates; refer to Daley et al. (2001) for details. The IACS and RMRS rules adopt the conventional *roof-top*-type mechanism model and rigid-plastic analysis of a partially loaded rectangular plate, where the load patch has dimensions of width ($s$) and height ($b$).

The focus of this study will be placed on the ice load models that underlie the ice load formulations in the IACS Unified Requirements and RMRS Rules (i.e., the ice pressure in the bow sub-region and the load patch height). A discussion regarding the model and assumptions that underlie shell plating requirements can be found in Hong and Amdahl (2007).

### *2.1 IACS ice load model*

This section describes the methodology used to determine the ice load formulation of the IACS Unified Requirements (Sec. I2.3).

*Notation*

| | |
|---|---|
| $p_{IACS}$ | IACS' ice crushing pressure |
| $p_{cr}$ | ice crushing pressure in accordance with Sanderson's pressure-area relationship |
| $b_{IACS}$ | height of the load patch |
| $P_o$ | ice strength factor in Sanderson's pressure-area relationship |
| $A$, $A_{red}$ | nominal and reduced contact area, respectively |
| $M_n$ | ship's mass accounting for the direction of the collision |
| $V_n$ | ship's speed at the moment of impact, along the collision normal |
| $\beta$ | normal frame angle which is measured in accordance with IACS (I2.3.2.1) |
| $\varphi$ | ice edge opening angle |
| $AR$ | aspect ratio |
| $h_i$ | ice thickness |
| $\sigma_i$ | ice flexural strength |
| $w_{IACS}$ , $W$ | width of the load patch |

| | |
|---|---|
| *ex* | exponent in Sanderson's pressure-area relationship |
| $Q_{IACS}$ | ice crushing force at the end of the interaction |
| $q_{IACS}$ | line load of IACS |
| *wex* | characteristic of ice edge spalling |

For ships that operate in Arctic and Antarctic waters, the design scenario is a glancing impact on the bow with an ice floe of infinite mass (Figure 1a). Ice crushing loads are characterized by an average pressure ($p_{IACS}$) that is uniformly distributed over a rectangular load patch of height ($b_{IACS}$) and width ($w_{IACS}$) (Equations 1a–1c).

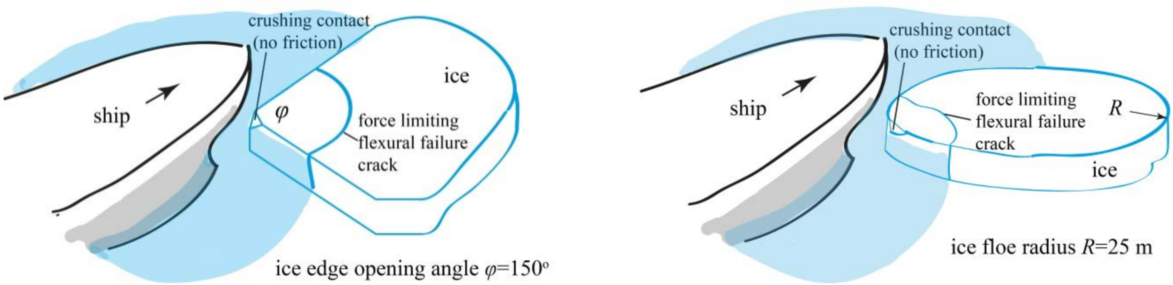


(a) impact against an ice floe with an angular edge (Daley, 2000)

(b) impact against an ice floe with a rounded edge

Figure 1. Design scenarios in the (a) IACS Unified Requirements and (b) RMRS Rules.

$$p_{IACS} = P_o^{\frac{1+2wex}{3+2ex}} AR^{1-wex} \left( \frac{\tan(\varphi/2)}{\cos(\beta)^2 \sin(\beta)} \right)^{\frac{1+ex-wex}{3+2ex}} \left( \frac{3+2ex}{2} M_n V_n^2 \right)^{\frac{2(1+ex-wex)}{3+2ex}} \quad \text{1a}$$

$$b_{IACS} = P_o^{\frac{-wex}{3+2ex}} AR^{\frac{wex}{2}-1} \left( \frac{\tan(\varphi/2)}{\cos(\beta)^2 \sin(\beta)} \right)^{\frac{wex}{2(3+2ex)}} \left( \frac{3+2ex}{2} M_n V_n^2 \right)^{\frac{wex}{3+2ex}} \quad \text{1b}$$

$$w_{IACS} = b_{IACS} \cdot AR \quad \text{1c}$$

These formulae are based only on the crushing failure of ice. The loads are governed by the available kinetic energy. A single load value ($Q_{IACS} = p_{IACS} \cdot b_{IACS} \cdot w_{IACS}$) at the end of the interaction is considered; this value corresponds to the maximum hull-ice contact area that is developed. The method assumes that a ship-ice collision has a short duration, such that the six-degrees-of-freedom (6 DOF) problem can be modeled by an equivalent 1-DOF model in which all motions between the ship and the ice are normal to the ship's side at the collision point. Frictional forces are disregarded. An energy-based approach proposed by Popov et al. (1967) is adopted for the ice load. The kinetic energy of the ship is equated to the ice-crushing energy, which is determined by integrating the ice force over the penetration depth. The ice force is calculated by integrating the ice crushing pressure ($p_{cr}$) over the nominal contact area ($A$). A Sanderson-type process pressure-area relationship is assumed (Sanderson, 1988):

$$p_{cr} = P_o A^{ex}, \quad \text{(2a)}$$

or in its alternative formulation:

$$p_{cr} = P_o \left( \frac{A}{A_0} \right)^{ex}, \tag{2b}$$

where $A_0$ is the reference contact area ($A_0$=1.0 m$^2$), $P_o$ is the ice strength factor, and the exponent $ex$ is a constant ($ex$<0), i.e., the average pressure decreases with the nominal (projected) contact area.

For an angular ice floe, the nominal contact area ($A$) is triangular-shaped. To simplify the calculations, a rectangular contact area (load patch) with the same aspect ratio ($AR$) is used. The effect of local ice edge fractures (spalls) is treated by assuming a reduction in the size of the nominal contact area while maintaining a constant aspect ratio and total force. This reduction in size is given by the following equation:

$$A_{red} = \frac{A^{wex}}{AR^{1-wex}}, \text{ where } AR = 2 \cdot \tan(\varphi/2) \cdot \sin(\beta). \tag{3}$$

At the end of the collision, i.e., when all kinetic energy is dissipated by ice deformation, the ice crushing pressure ($p_{IACS}$), height ($b_{IACS}$) and width ($w_{IACS}$) of the load patch are given by Equations 1a–1c.

Furthermore, it is argued that the ice crushing force (and thus the average pressure) cannot exceed the force (average pressure) required to cause the ice to fail because of bending; hence, the values of $p_{IACS}$, $b_{IACS}$ and $w_{IACS}$ are restricted to be less than some fixed values that are determined from the bearing capacity of an infinite ice plate under a concentrated load. In this context, two additional ice parameters are introduced, i.e., the ice flexural strength ($\sigma_f$ )

and ice thickness ($h_i$). Accounting for bending ice failure, Equations 1a and 1b can be rewritten as:

$$p = f_1(\varphi, ex, P_o, V_n, \beta, wex) \cdot f_2(\beta, \sigma_f, h_i) \cdot M_n^{0.14} \text{ and} \tag{4a}$$

$$b = f_3(\varphi, ex, P_o, V_n, \beta, wex) \cdot f_4(\beta, \sigma_f, h_i) \cdot M_n^{0.25}. \tag{4b}$$

Here, the terms $f_1$ and $f_3$ represent contributions due to ice crushing along the line of collision (Equations 1a and 1b), and $f_2$ and $f_4$ account for ice failure due to bending, i.e., $f_2(\beta, \sigma_f, h_i) < 1.0$ and $f_4(\beta, \sigma_f, h_i) < 1.0$. When $f_2 = f_4 = 1.0$, only ice crushing is considered. The calculated pressure and the load height are functions of the ice geometry and its mechanical characteristics (i.e., $\varphi$, $h_i$ , $ex$, $wex$, $P_o$ and $\sigma_f$ ), the geometry of the vessel, and its speed and mass (i.e., $\beta$, $V_n$, and $M_n$). The subscript $n$ indicates a reduced value that accounts for the orientation of the collision.

The IACS approach assigns a characteristic value to $\varphi$, $ex$, and $wex$ ($\varphi$ = 150°, $ex$ = –0.1 and $wex$ = 0.7), whereas the ship speed, ice thickness and ice strength parameters ($V$, $h_i$ , $P_o$ and $\sigma_f$) are assumed to be ice class dependent. Each class factor is developed from values for ice strength characteristics and ship speeds, whereas the ice constants ($ex$ and $wex$) are included in the exponents of the terms within the expression for design ice pressure and for design load height, respectively; see Table 1. Consequently, for each ice class, the design loads, pressure and size of the load patch are functions of the hull angles and vessel displacement. The ice class factors (e.g., crushing ice factor $CF_C = P_0^{0.36} \cdot V^{1.28}$) are selected to give values that are consistent with the range of desired class requirements for strength (i.e., PC1 should require plate and framing dimensions consistent with the highest Arctic ice classes in service).

### *2.2 RMRS ice load model*

The RMRS rules originate from rules suggested during the late 19th century and beginning of the 20th century. Since then, ice load calculation methods have evolved; see Kalenchuk and Kulesh (2010) for details. However, it is believed that this ice load model has not been described in the publicly available literature (IMO, 2014). This section presents an overview of the scientific basis for the RMRS ice load formulations (RMRS Vol. 1 Pt. 2 Sec. 3.10). A closed-form solution that links the rule-based ice loads and physics is given in the Appendix. The overview is based on the following literature and focuses on loads due to ice crushing failure:

1) The solution by Kurdyumov and Kheisin (1974) and Kurdyumov et al. (1980) for an impact against a large ice floe with a rounded ice edge.
2) The solution by Kurdyumov and Kheisin (1976) for an impact between an ice wall and a spherically shaped indenter.
3) The description of a methodology for the ice-strengthening requirements for ice-going vessels given in Appolonov et al. (1996).
4) The description of modifications proposed for the Kurdyumov and Kheisin hydrodynamic model of ice crushing (Appolonov et al., 2002 and Appolonov et al., 2011).

Note that the work of Kurdyumov and Kheisin (1976) is often referred to in the context of ship design, (although the solution presented therein is not for the RMRS design scenario). Instead, their model is for indentation into an ice wall by a spherically-shaped indenter. An impact against an ice floe with a rounded edge (the RMRS scenario) was solved by Kurdyumov and Kheisin (1974) and Kurdyumov et al. (1980), although these works are rarely referenced outside Russia.

*Notation*

| | |
|---|---|
| $u_x, u_y, u_z$ | velocity components of crushed ice particles in the intermediate layer |
| $\mu$ | dynamic viscosity of crushed ice in the intermediate layer |
| $u_{pn}(t)$ | penetration speed (ice crushing speed) in the direction of indentation |
| $h(x,t)$ | thickness of the intermediate layer |
| $\bar{x} = x / b_{eff}$ | dimensionless coordinate $\bar{x} \in [-1;1]$ |
| $sp = b_0 / b_{eff}$ | coefficient accounting for edge spalling effects |
| $A$ | contact area |
| $M_n$ | ship's mass accounting for the direction of the collision |
| $V_n$ | ship's speed at the moment of impact, accounting for the orientation of the collision |
| $2a$ | width of the contact area |
| $c = 2b_0$ | height of the contact area |
| $\bar{v} = v/a$ | dimensionless coordinate $\bar{v} \in [-1;1]$ |
| $\zeta$ | penetration depth measured along the direction of indentation |
| $a_p$ | $a_p = (6\mu k_p^3)^{5/24}$, the ice strength factor |
| $b_{HDM}$ | load height in accordance with the HDM |

| | |
|---|---|
| $q_{HDM}$ | line load in accordance with the HDM |
| $b_0$ | half-height of the contact zone |
| $b_{eff}$ | effective half-height of the contact zone |
| $k_p$, $n$ | parameters of the relationship between the ice pressure and the thickness of the crushed layer |
| $M$ | ship displacement |
| $V$ | ship forward speed at the moment of impact |
| $Q_{HDM}$ | total contact force along the line of collision, in accordance with the HDM |
| $R$ | ice floe radius |
| $\beta$ | frame angle which is measured in accordance with Figure 2 |
| $p_{HDM}$ | ice crushing pressure in accordance with the HDM |

The approach presented in Kurdyumov and Kheisin (1974, 1976) and Kurdyumov et al. (1980) is often referred to as the Kurdyumov-Kheisin model or HDM for a solid body impact against ice (Likhomanov et al., 1998 and Appolonov et al., 2011). The RMRS ice pressure formulation is based on this methodology (Appolonov et al., 1996).

The method addresses the loads that act on the hull during impact with a large ice floe with a rounded edge (Figure 1b). The energy-based approach of Popov et al. (1967) is adopted for the ice load. The kinetic energy of the ship is equated to the crushing energy of the ice, which is determined by integrating the ice force over the penetration depth. The ice force is calculated by integrating the ice crushing pressure ($p_{HDM}$) over the contact area ($A$) and accounts for ice edge spalling effects. In contrast with the IACS formulation, the pressure is determined by assuming that there is an intermediate layer of crushed ice between the hull and the solid (undamaged) ice (Figure 2). The pressure is proportional to the thickness of the intermediate layer ($h$):

$$p_{HDM}(x,t) = k_p \cdot h(x,t)^n \quad (5)$$

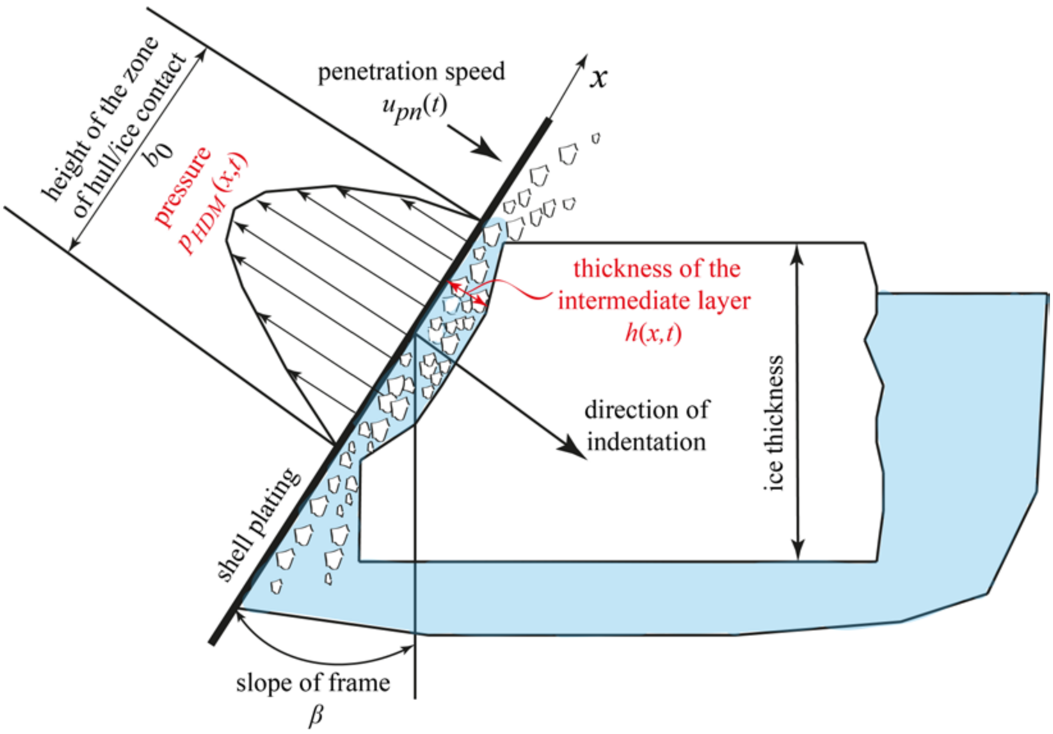


Figure 2. Illustration of ice edge crushing for contact between a ship's side and ice, in accordance with the Kurdyumov and Kheisin model.

The model treats the intermediate layer as an incompressible viscous fluid, and simplified Navier-Stokes equations are used to derive the ice pressure. Frictional forces between the ship's side and the crushed layer are disregarded. The solution becomes

$$p_{HDM}(x,t) = \left( \frac{3}{2}\frac{n+3}{n}\mu u_{pn}(t) k_p^{\frac{3}{n}} (sp^2 - \overline{x}^2) \left( \frac{b_0}{sp} \right)^2 \right)^{\frac{n}{n+3}}, \tag{6}$$

where the penetration speed ($u_{pn}$) is determined from energy balance and accounts for ice edge spalling effects:

$$u_{pn} = \left\{ V_n^{\frac{n+6}{n+3}} - \left( \frac{n+6}{n+3} \right) \left( \frac{2n+6}{9n+15} \right) \frac{\left( \frac{3}{2}\frac{n+3}{n}\mu k_p^{\frac{3}{n}} \right)^{\frac{n}{n+3}}}{M_n \cos^{\frac{7n+9}{2n+6}}\beta \cdot \sin^{\frac{3n+3}{n+3}}\beta} J_1 J_2 \zeta^{\frac{9n+15}{2n+6}} \right\}^{\frac{n+3}{n+6}}, \tag{7}$$

where $J_1$ and $J_2$ are numerical factors that account for ice edge spalling effects and hull-ice contact shape deviations from a rectangle, i.e.,

$$J_1 = 2^{-\frac{2n}{n+3}} \cdot sp^{-\frac{3n+3}{n+3}} \cdot \int_0^1 \left( sp^2 - \overline{x}^2 \right)^{\frac{n}{n+3}} d\overline{x} \text{ and } J_2 = 2\int_0^1 \left( 1 - \overline{v}^2 \right)^{\frac{3n+3}{n+3}} d\overline{v}.$$

The pressure (Equation 6) varies over the contact area, with a maximum at the center of the contact area. At a certain penetration depth, the maximum pressure has a peak ($p_{peak}$). The model of Kurdyumov and Kheisin assumes a linear relationship between the pressure and thickness of the crushed layer ($n$=1 in Equation 5). Accounting for bending (or buckling of ice), $p_{peak}$ can be written as follows:

$$p_{peak} = 0.662(V)^{\frac{13}{24}}(M)^{\frac{1}{6}} a_p (2R)^{-\frac{1}{12}} F_p f_p \, , \tag{8}$$

where $F_p$ is a hull shape factor and $f_b$ is a pressure-limiting factor. The constant 0.662 accounts for spalling of ice edges ($sp$=1.06).

The load height ($b_{HDM}$) is determined from the condition $u_{pn} = 0$ and accounts for the geometry of the hull-ice contact and spalling of ice edges:

$$b_{HDM} = 1.344(V)^{\frac{7}{12}}(M)^{\frac{1}{3}}(a_p)^{-\frac{2}{5}}(2R)^{-\frac{1}{6}} F_b f_b \, . \tag{9}$$

Here, $F_b$ is a hull shape factor and $f_b$ is a height-limiting factor. Both $F_p$ and $F_b$ (Equation 8 and 9) account for the eccentricity of the impact and are derived using the methodology described in Popov et al. (1967) and in Daley (2000). The limiting factors $f_b$ and $f_p$ ($f_p < 1.0$ and $f_p < 1.0$) account for bending (or buckling) ice failure at lower load levels.

Analogous to Equations 4a and 4b, Equations 8 and 9 can be rewritten as functions of the ice floe geometry, mechanical properties of the crushed layer, ship speed and vessel displacement:

$$p_{peak} = g_1(R,\mu,k_p,V_n,\beta,sp)\cdot g_2(\beta,\sigma_f,h_i)\cdot M_n^{0.17} \text{ and} \tag{10a}$$

$$b_{HDM} = g_3(R,\mu,k_p,V_n,\beta,sp,)\cdot g_4(\beta,\sigma_f,h_i)\cdot M_n^{0.33}. \tag{10b}$$

Note that the exponents of $M_n$ in Equations 10a and 10b (see also Table 1, Column "RMRS") are strictly valid for $n$ = 1.0 (see Equation 5). The design pressure and size of the load patch (Table 1) are functions of the hull angles in the considered sub-region and the vessel displacement. $F_p$ (Equation 8) is approximated by the shape factor $v_m$ (Table 1), and $F_b$ (Equation 9) is approximated by $u_m$. Each RMRS class factor (i.e., $a_1$ and $C_1$) is developed from the values for ice parameters (i.e., $R$, $\mu$, $k_p$, $sp$, $\sigma_f$, and $h_i$) and the ship's forward speed at the moment of impact; operational experience is used to determine these values. These values and the explicit model that links the class factors to the ice parameters are not included in the scientific documentation of the rules (i.e., Appolonov et al., 1996).

## *3 Discussion*

This section has rigorously a scientific objective. We have considered the rationale of IACS and RMRS ice loads and also the specific assumptions underlying the Daley and Kurdyumov-Kheisin models of ice crushing.

It should be acknowledged that the two rules share much in common. In both rules, the requirements of shell plating thickness are based on a loading event (i.e., a glancing impact with an ice edge) that begins with ship-ice edge contact over a small area, and continues with growing contact area until the entire structural grillage is loaded to its design condition. Both rules use ice pressures to develop a formulation for ice collision force and adopt the energy principles proposed by Popov et al. (1967).

The advantage of the IACS overall framework is that a detailed derivation of the design loads can be found in the literature, along with the list of assumptions for linking the ice class factors to physical values, such as the ice flexural strength and ice thickness; see Daley (2000) for more details. The RMRS design formulae can be difficult to understand because explicit relationships between the physical parameters and class factors are not available in the open literature. However, a qualitative comparison of the IACS and RMRS approaches can be made (see Section 3.4).

We are still a long way from being able to formulate ship rules strictly from theory. The Daley model and the Kurdyumov and Kheisin model for calculating ice crushing pressures lack some physical realism, thus making their use difficult outside the application range of the rules. The drawback of these models is that some unsupported assumptions are introduced (e.g., the dynamic viscosity, pressure distribution over the contact area, characteristics of ice edge spalling and a relationship between the crushed layer thickness and the pressure). Within this context, it is interesting to evaluate the assumptions that underlie the ice crushing models based on the current understanding of the ice-structure interaction process and to test the sensitivity of the results for both models with respect to uncertainties in the input values.

## *3.1 Assumptions regarding the pressure-area relationship and ice pressure distribution*

### *3.1.1 Daley's load model and the IACS Unified Requirements*

Equation 2a (or 2b) implies that the average pressure over the full contact area (or nominal area) always decreases with increasing nominal contact area. This trend of decreasing pressure with increasing contact area has been accepted by the international ice engineering community. Several explanations for the pressure-area relationship (Equation 2a) have been offered. For details, see Kim and Schulson (2015), Palmer and Sanderson (1991), Palmer et al. (2009), Sanderson (1988) and Schulson and Duval (2009). However, the hypothesis that the average pressure depends primarily on the contact area is not universally accepted (Dempsey et al., 2001; Timco and Sudom, 2013). Factors other than the area, such as the ice type, loading rate (or ice penetration speed), aspect ratio, surrounding ice extent, and ice failure mode, may influence the average pressure. A comprehensive analysis of experimental data from structures in ice-covered waters (Timco and Sudom, 2013) has demonstrated that in many cases, these factors are more important than the area itself. For example, the coefficient $P_o$ and the exponent $ex$ are functions of the ice failure mode and loading rate (Timco and Sudom, 2013), and there exists a functional relationship between the coefficient $P_o$ and the radius of the indenter (Kim and Schulson, 2015).

The pressure in Equations 2a (or 2b) is a function of many variables (i.e., not only the contact area), although these variables (e.g., ice type and floe size) are contained in $P_o$ (or $ex$) and define a single design point for each ice class. $P_0$ (Equation 2b) is a class-dependent parameter that shall be understood as the ice pressure over 1.0 m$^2$. The exponent $ex$ is always –0.1 (Daley, 2000).

The constant $ex$ is –0.1 for all ice classes. This assumption implies that there is a knowledge gap. Why is $ex$ assumed to be independent of the vessel speed, which varies for different ice classes? One may speculate that during an impact, the interaction speed will vary from $V_n$ to 0.0, whereas the nominal contact area will increase. The exponent $ex$ will also vary during an impact. For example, at the beginning of the interaction at speeds near $V_n$ ($V_n$ is large enough to impart brittle behavior), brittle failure mechanisms (which are governed by crack initiation, growth and interaction) will dominate; the average pressure over the nominal area will decrease with increasing nominal area ($p_{cr} \sim A^{ex}$, where $-0.7 \leq ex < 0$). At the end of an impact (the ship's speed is approximately 0.0), ductile behavior (which is governed by a combination of mechanisms, including recrystallization, grain boundary sliding, and dislocation creep) will dominate. Correspondingly, the crushing pressure will be nearly constant and independent of area ($p_{cr} \sim A^0$), and Sanderson's pressure-area relationship no longer applies.

### *3.1.2 Kurdyumov-Kheisin's HDM and the RMRS Rules*

The HDM accounts for a non-uniform pressure distribution over the full global ice contact area, assuming a linear proportionality between the pressure and intermediate-layer thickness ($n$ = 1 in Equation 5). The dynamic viscosity ($\mu$) and proportionality constant ($k_p$) are required. These two parameters are often combined into a single ice crushing factor $a_p = (6\mu k_p^3)^{5/24}$ with a unit of $\mathrm{Pa}^{5/6}\cdot(\mathrm{s/m}^3)^{5/24}$. The value of this factor cannot be measured directly; instead, the value is back-calculated from tests. The value ranges between $a_p \approx (133\cdot10^3–424\cdot10^3)$ $\mathrm{Pa}^{5/6}\cdot(\mathrm{s/m}^3)^{5/24}$ for freshwater spring ice and $a_p \approx (510\cdot10^3–909\cdot10^3)$ $\mathrm{Pa}^{5/6}\cdot(\mathrm{s/m}^3)^{5/24}$ for winter freshwater lake ice (Tunik, 1987). Figure 2 shows the contact geometry and pressure distribution over the height of the hull-ice contact zone. The pressure was calculated using Equation 6 for various values of $n$. Note that $n$ = 1.0 is used in the HDM/RMRS analytical procedure for determining ice loads in the bow region.

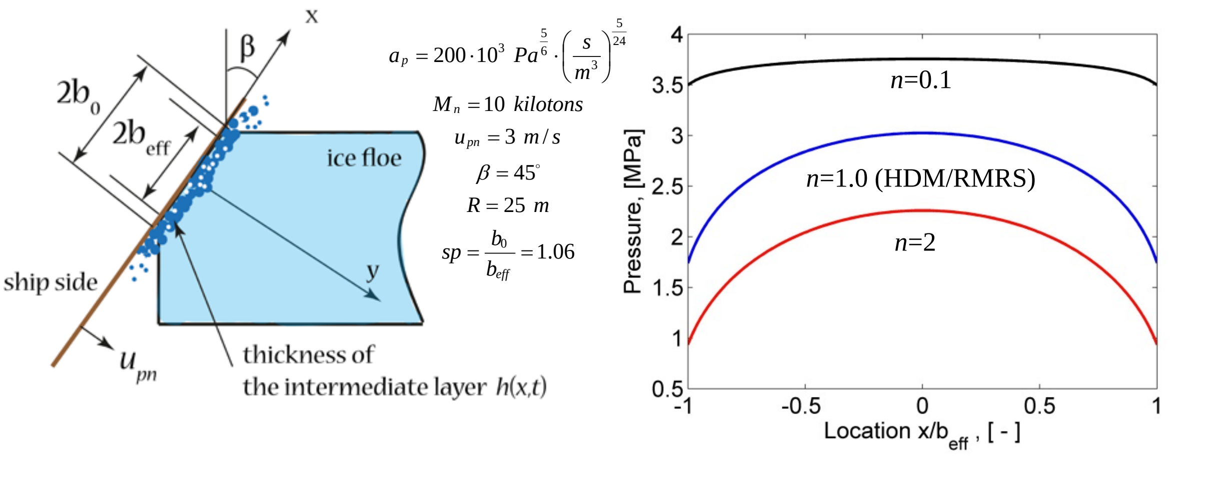


(a) (b)

Figure 2. The HDM: (a) schematics of the impact problem and (b) calculated local distributions of the pressure along $x$ for $b_0 = 1.0$ m.

The calculated pressure profiles are symmetric and attain maxima at the center of the contact region ($x/b_{eff} = 0$). The pressures vanish at $x = \pm b_0$.

There are two drawbacks to the HDM. The first drawback is that the pressure maximum is less pronounced than that in the measured pressure data; see, e.g., Daley's (2004) schematic representation of pressure distributions over a contact height. Many experimental observations and measurements during brittle ice crushing (Jordaan, 2001 and Sodhi, 2001) indicate a common feature: the presence of localized high-contact-pressure zones or line-line zones (Joensuu and Riska 1989). Observations and measurements suggest a bell-shaped pressure profile, whereas the HDM model predicts a parabolic pressure distribution (Figure 2b). The second drawback is the assumption of a direct proportionality between the pressure and intermediate layer thickness, i.e., $n$ = 1.0 (Equation 5). Experimental evidence suggests that the pressure in the contact zone has a pronounced maximum in the direct contact area, which is relatively narrow compared with the nominal (projected) contact area. The maximum pressure occurs in areas in which the intermediate layer is thin, although the HDM assumes otherwise.

These two drawbacks have been recognized; consequently, several modifications to the HDM have been proposed. For additional details, refer to Appolonov et al. (2002) (in Russian) or Appolonov et al. (2011) (in English). One of the suggested modifications is to replace Equation 5 (which conflicts with experimental data) by a system of additional conditions that account for the actual characteristics of the pressure pattern's maximum. Another proposal is to introduce an effective contact area; the pressures are considered constant within this area and zero otherwise. The latter proposal has been supported by comparisons with experimental data. It should be noted that for the modified versions of the HDM, closed-form solutions have not been provided in the open literature. This fact limits the practical use of the proposed modifications.

### *3.2 Ice spalling assumptions*

Both the IACS and HDM/RMRS approaches account for ice edge spalling that occurs during brittle crushing. In the IACS approach, ice edge spalling is treated by reducing the size of the load patch (Equation 3) while maintaining a constant force and aspect ratio. Scant reasoning behind the selected value for *wex* has been provided. Below, it is demonstrated that the assumption of a constant value for *wex* (i.e., 0.7) in Equation 3 has a substantial effect on the ice pressure values.

To account for edge spalling in the HDM, a spalling factor $sp = b_0/b_{eff}$ ($sp > 1.0$) is introduced. The expression for the line load ($q_{HDM}$) as a function of the penetration depth ($\zeta$) is

$$q_{HDM}(\zeta) = \int\limits_{2b_{eff}} p_{HDM}(b_0^{\;2} - x^2, \zeta)dx \xrightarrow{x=b_{eff}\cdot\bar{x},\bar{x}\in[-1\;1]} q_{HDM}(\zeta) = \int\limits_{2} p_{HDM}(sp^2 - \bar{x}^2, \zeta)d\bar{x}\,. \quad (11)$$

Details of the derivation and an illustration, which shows the geometry of the impact problem, can be found in the Appendix. Note that a value of $sp$ = 1.06 is used in the HDM. An empirically based value of $sp$ = (1.05–1.08) was reported in Kurdyumov and Kheisin (1976) for the case of a solid ball impacting an ice wall. There are limited experimental data for ship-shaped structures that could be used to further assess the physical plausibility of the chosen constants (i.e., *sp* and *wex*). For the IACS and HDM/RMRS design scenarios, no explicit validations of *wex* and *sp* are available in the open literature; thus, experiments should be conducted to improve the basis for these constants.

In summary, the ice load models underlying the IACS and RMRS rules include three parameters that are not well known, i.e., $P_o$, $ex$ and $wex$ in the IACS rules and $n$, $a_p = f(k_p, \mu)$, and $sp$ in the HDM/RMRS approach. In the IACS and RMRS rules, these parameters were selected based on the existing operational experience to yield a sufficiently safe and robust vessel, i.e. to give the requirements that are consistent with the range of desired strength requirements. When the experience is limited, or when one decides to use the ice load models outside the application range of the ship rules, it will be necessary to test the sensitivity of the results of both methods to uncertainties in the input values.

### *3.3 Ramifications of the IACS and RMRS assumptions*

Ice crushing occurs at the edge that contacts a ship's side. As the penetration depth increases, the crushing force increases until failure due to bending. A closed-form solution that accounts for the combination of ice crushing and flexural failure does not exist. For simplicity, we limit the discussion to ice crushing failure because in both methods (the IACS and HDM/RMRS approaches), the highest ice pressures are associated with ice crushing failure.

Figures 3 and 4 present the results of a sensitivity study for the Daley model of ice crushing (used to develop the IACS rules) and the Kurdyumov and Kheisin HDM (used to develop the RMRS rules), respectively. In the calculations, the vessel displacement ($M_n$) was kept constant and equal to 10 kilotons. Only one parameter was varied at a time.

The maximum and minimum values for a varying parameter were determined based on available experimental and analytical data and engineering judgment. For example, regarding the ice floe opening angle ($\varphi$), Popov et al. (1967) calculated the magnitude of $\varphi$ by assuming the dimensions of the segments that were broken off by the icebreaker. Their calculations indicated that $\varphi$ can vary over a wide range, from 45° to 145°; average values between 90°

and 100° were recommended for calculations. In the IACS approach, $\varphi$ =150° is used. In this context, a sensitivity study for $\varphi$ = 90–150° was performed.

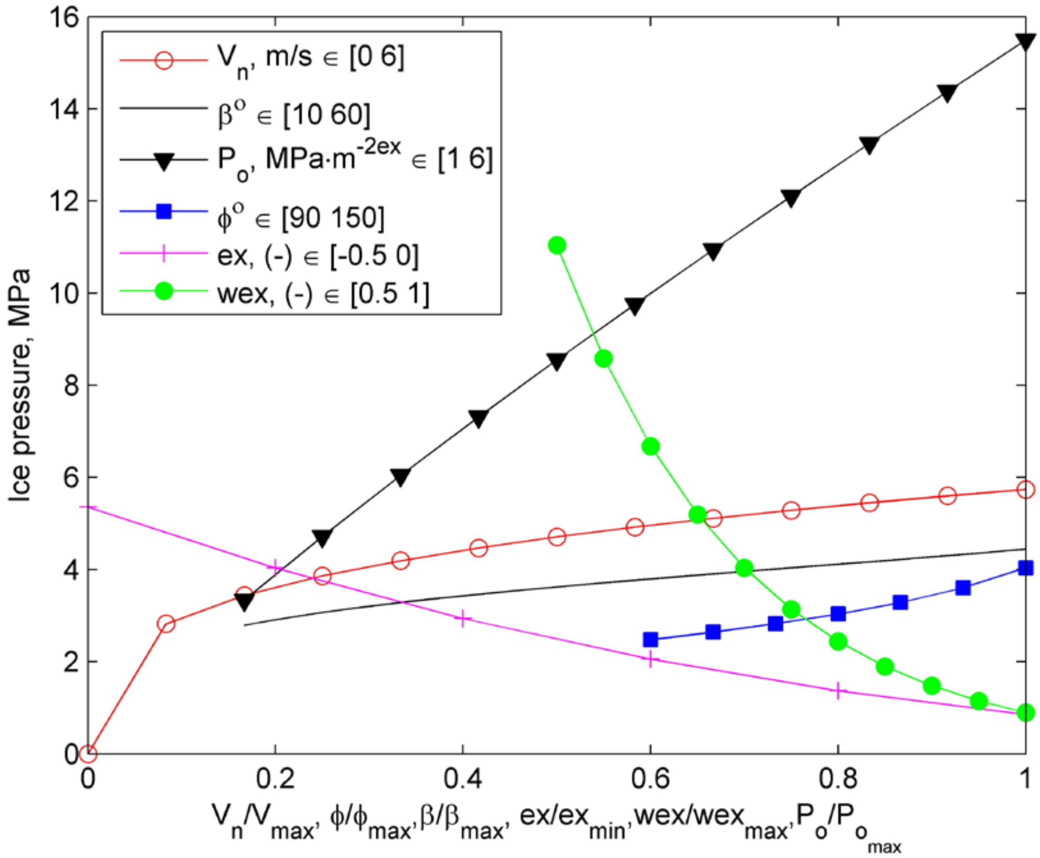


Figure 3. Effect of physical parameters on the ice pressure calculated using the Daley model of ice crushing.

Figures 3 and 4 show that the values of the exponent in the Sanderson pressure-area relationship (*ex*), spalling characteristic (*wex*) and ice strength factor ($a_p$) are the most important assumptions (especially *wex* and $a_p$). Unfortunately, these parameters are the most uncertain. This result clearly indicates a knowledge gap that must be addressed in the future.

The results from Daley's model (Figure 3) indicate a slight decrease in the ice crushing pressure with decreasing normal frame angles. This finding is the opposite of what one would expect during brittle crushing, i.e., an increase in local pressure values for steeper frame angles. Steeper frame angles will typically correspond to smaller aspect ratios and larger nominal contact areas at the end of the interaction, assuming that ship-ice interaction is governed by a Sanderson's pressure-area relationship and that the force is limited by available kinetic energy. When the nominal contact area increases, the pressure in high-pressure zones also increases. The same effect of ice thickness is also observed during brittle crushing (Dempsey et al., 2001).

The discussion above refers to the brittle ice crushing failure mode. The actual design values are limited by ice failure due to out-of-plane bending and are inversely proportional to the frame angle. For larger angles, ice fails because of bending at lower load levels, in agreement with observations of full-scale ship-ice interactions.

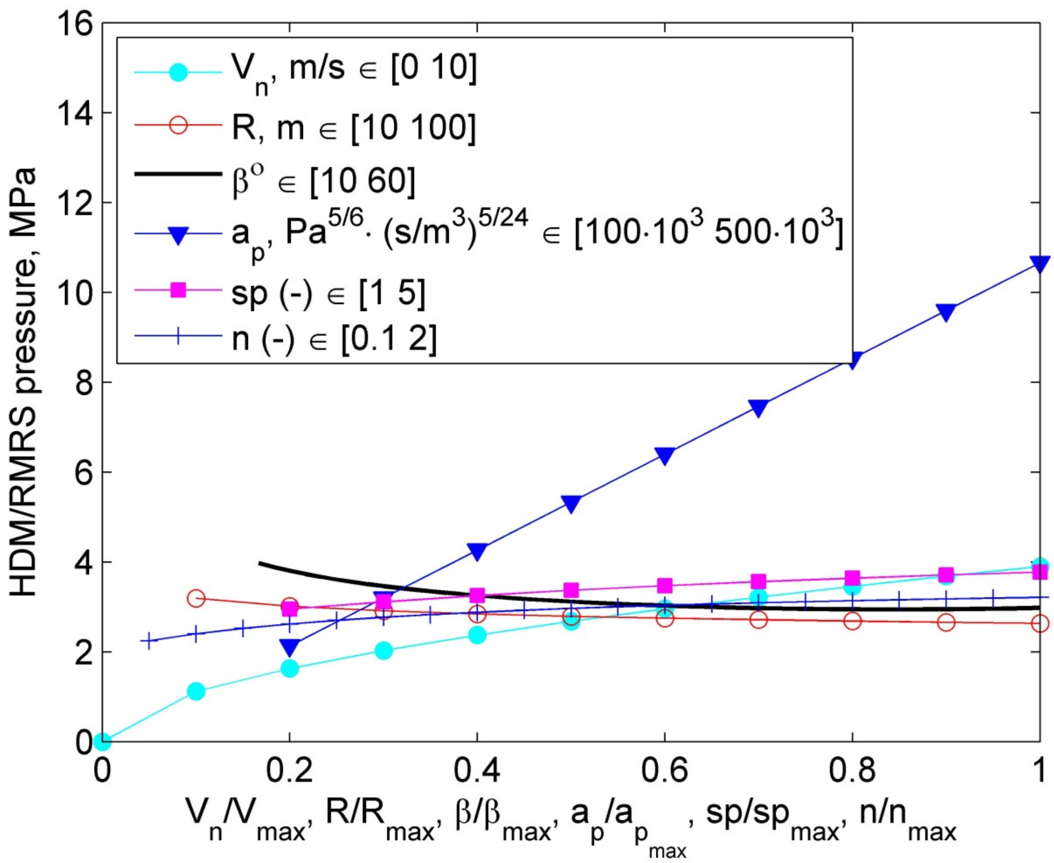

Figure 4. Effect of physical parameters on the HDM/RMRS pressure.

### 3.4 *A qualitative comparison between the IACS and HDM/RMRS ice crushing loads*

Figure 5 shows the evolution of the impact force, ice pressure and line load as a function of the penetration depth. These forces are generated by crushing failure of an ice floe with a rounded edge (the HDM/RMRS load model in Section 2.2) and a wedge-shaped ice edge (the IACS load model in Section 2.1). Table 2 provides a comparison between the two models, and Table 3 presents the results of the sensitivity study in Section 3.3.

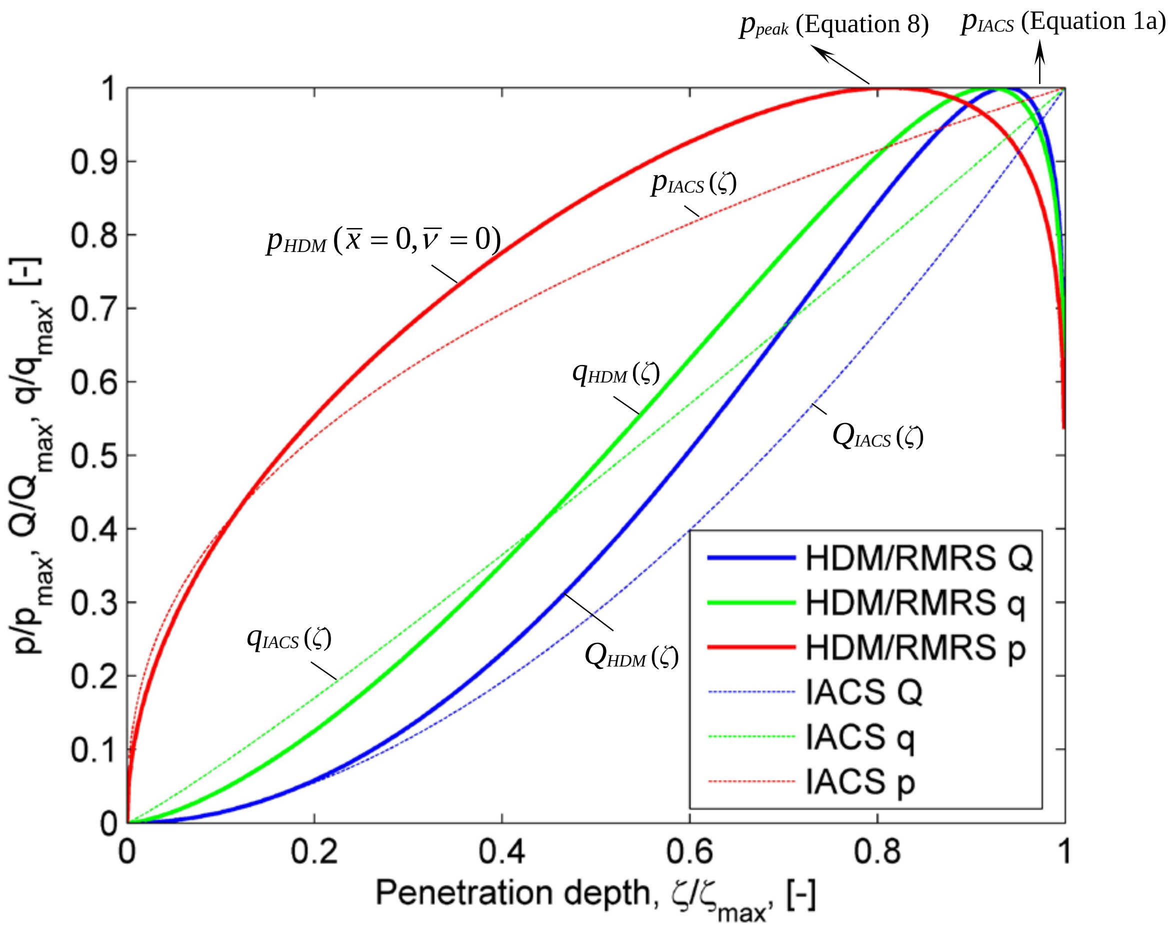

Figure 5. Load-penetration relationships determined according to the IACS load model (Section 2.1) and to the HDM/RMRS model (Section 2.2): $Q/Q_{\mathrm{max}}$ is the normalized total force, $q/q_{\mathrm{max}}$ is the normalized line load, $p/p_{\mathrm{max}}$ is the normalized ice pressure, and $\zeta/\zeta_{\mathrm{max}}$ is the normalized penetration depth.

As can be observed from Figure 5, $Q_{IACS}$, $q_{IACS}$ and $p_{IACS}$ increase with penetration depth in the IACS calculations and attain their maximum values at the end of an impact, i.e., when $\zeta = \zeta_{\mathrm{max}}$. In the IACS approach, a single load value at the end of an interaction ($\zeta = \zeta_{\mathrm{max}}$) is considered when deriving the ice pressure (Equation 1a) and load patch size (Equations 1b and 1c). Expressions for calculating the impact duration were not provided in Daley (2000).

In the HDM/RMRS formulation, the maximum values are reached before a vessel comes to a complete stop. The maximum penetration depth ($\zeta_{\mathrm{max}}$) can be determined from Equation 7 by setting $u_{pn} = 0$ (refer to the Appendix for details). The peak pressure (Equation 8) is reached before the maximum force is attained. The expression for calculating the impact duration is provided in Kurdyumov and Kheisin (1974). The normalized parameters $p_{HDM}/p_{max}$, $q_{HDM}/q_{max}$ and $Q_{HDM}/Q_{max}$ as functions of $t/t_{max}$ ($t_{max}$ is the duration of the impact) resemble those in Figure 5, although there is a slight shift to the left. The shape of the HDM total force and time histories resembles that measured experimentally during collisions with ice. It is also realistic that the HDM pressure at the center of the contact area, i.e., $p_{HDM}(\overline{x} = 0, \overline{\nu} = 0)$ increases with increasing penetration depth.

Figure 5 indicates that $p_{HDM}(\overline{x} = 0, \overline{\nu} = 0)$ begins descending towards zero after reaching a peak ($p_{peak}$). The extent of this decrease is debatable because at this stage, the indentation speed is almost zero and the nominal contact area is large; and thus, the ice response can be macroscopically ductile and governed by compressive ice strength. This means that $p_{HDM}(\bar{x}=0,\bar{v}=0)$ will not necessarily decrease but will rather be nearly constant.

Table 2. Functional dependencies of the ice crushing pressure and load height.

| Parameter | IACS | HDM/RMRS |
|---|---|---|
| Ice pressure ($p$) | $p_{IACS} = f_1(\varphi^*, ex^*, P_o^*, V_n^*, \beta, wex^*) \cdot M_n^{0.14}$ | $p_{peak} = g_1(R^*, a_p^*, n^*, V_n^*, \beta, sp^*) \cdot M_n^{0.17}$ |
| Load height ($b$) | $b_{IACS} = f_2(\varphi^*, ex^*, P_o^*, V_n^*, \beta, wex^*) \cdot M_n^{0.25}$ | $b_{HDM} = g_2(R^*, a_p^*, n^*, V_n^*, \beta, sp^*) \cdot M_n^{0.33}$ |

Asterisk symbol denotes factors for which ship owners or operators have no choice in what value to use

Table 2 demonstrates similarities and differences between the IACS and HDM/RMRS formulations for the ice crushing pressure and load height. Both rules specify a particular design scenario (i.e., an oblique impact with a large ice floe) as the design basis and use the energy-based approach proposed by Popov et al. (1967) to calculate ice loads. Each rule set assumes that the ice pressure and the load height are a function of the following parameters:

– *Ice geometry*, i.e., the floe angle in the IACS approach and floe radius in the HDM.
– *Ice mechanical characteristics*: in the IACS approach, these characteristics are the exponent in the Sanderson pressure-area relationship (*ex*), the spalling parameter (*wex*) and the ice strength factor ($P_o$). In the HDM, these characteristics are $a_p$ and $n$, where $a_p$ depends on the dynamic viscosity of the crushed ice in the intermediate layer ($\mu$) and a proportionality constant between the layer and the ice pressure ($k_p$).
– *Parameters of the vessel*, i.e., the ship speed at the moment of impact, ship mass (i.e., ship displacement) and hull shape.

Note the similarities and differences between the exponents of the vessel displacement. Despite the fact that the IACS and RMRS rules are based on completely different sets of assumptions, the functional dependencies of the pressure and load height on the vessel displacement are remarkably similar. The RMRS formulation has a slightly stronger dependency of the pressure and the load height on the vessel displacement, i.e.,

$$\frac{p_{RMRS}}{p_{IACS}} \propto M^{1.2} \text{ and } \frac{b_{RMRS}}{b_{IACS}} \propto M^{1.3}. \quad (12)$$

The main difference between the two approaches is that the IACS pressure is *the pressure averaged over the design load patch area*, whereas the RMRS pressure is *the maximum pressure at the center of the loaded area*. The IACS approach utilizes the Sanderson empirical pressure-area relationship, in which the average pressure decreases with increasing nominal contact area, whereas the RMRS approach assumes an intermediate crushed layer and uses the simplified Navier-Stokes equations to determine the pressure.

Table 3. Qualitative results of a sensitivity study.

| **Daley's model of ice crushing (used by IACS)** | | **Kurdyumov and Kheisin HDM (used by RMRS, *n*=1.0)** | | |
|---|---|---|---|---|
| **Effect** | **Ice crushing pressure** | **Effect** | **Impact duration/maximum penetration** | **Ice crushing pressure** |
| speed $V_n$↑ | ↑ | speed $V_n$↑ | ↑ | ↑ |

| | | | | |
|---|---|---|---|---|
| floe angle $\varphi$↑ | ↑ | floe radius $R$↑ | ↓ | ↓ |
| frame angle $\beta$↓ | ↓ | frame angle $\beta$↓ | ↓ | ↑ |
| spalling $wex$↑ | ↓ | spalling $sp$↑ | ↑ | ↑ |
| ice exponent $ex$↑ | ↓ | dynamic viscosity of the intermediate layer $\mu$↑ | ↓ | ↑ |
| ice 'strength' $Po$↑ | ↑ | crushed layer strength $k_p$↑ | ↓ | ↑ |

Table 3 indicates that some of the results obtained by both models in the presence of uncertainty in the input parameters show similar trends (e.g., an increase in ice crushing pressures with increasing impact velocities), whereas some are debatable. For example, refer to the effect of the frame angle that was discussed in Section 3.3. Other important (or debatable) effects are related to the floe radius and the ice spalling parameter, which are discussed in more detail below.

*Effect of the floe radius*

The HDM predicts the opposite of what one would expect, i.e., an increase in ice pressure for ice floes with larger radii. Consider two impacts, one with an ice floe with radius $R_s$ and another with $R_l > R_s$. If the speed of impact is large enough to impart brittle ice behavior, the pressure is expected to be higher for the larger floe because the ice in the middle of the contact zone is more confined. This notion is analogous to the effect of ice thickness during brittle crushing (Dempsey et al., 2001), i.e., as ice thickens, the peak pressures observed in high-pressure zones increase.

The maximum penetration distance (and impact duration) becomes shorter with increasing floe radius (Table 3), which is physically plausible because the confined ice (in the case of larger radius ice floes) can dissipate more energy during crushing, thereby resulting in shorter impact times.

*Effect of ice spalling*

The ice spalling constant (*wex*) is the most influential parameter in the Daley model of ice crushing. Higher *wex* values correspond to larger reductions in the contact area (Equation 3) and larger volumes of ice that brake off from the floe edge. In the IACS rules, this parameter is set to 0.7; a value of 1.0 would indicate no spalling. Figure 3 demonstrates that by varying *wex* between 0.5 and 1.0, pressure values that range from 1 to 12 MPa can be obtained. The lowest value was obtained for *wex* = 1.0, and the ice pressure increased with decreasing *wex*. From a physical perspective, this *wex* effect corresponds to a situation in which the pressure in the crushed and extruding ice adds a confining stress on the solid ice (high-pressure zone), thereby increasing the pressure in this high-pressure zone (Daley et al., 1998). In this context, the pressure determined using Equation 3 can be interpreted as the average pressure that accounts for direct hull-ice contact (or high-pressure zones) and contact with the crushed ice, where the crushed ice can extend from a high-pressure zone to the edge of the nominal contact area.

In the HDM, the parameter *sp* > 1 indicates ice spalling. Larger *sp* values are indicative of larger spalls (i.e., smaller actual contact areas). When *sp* = 1, no spalling occurs. In the RMRS approach, the spalling parameter has a larger value with a larger reduction in the contact area, which is the opposite case for the IACS approach. In accordance with the above discussion regarding *wex*, the ice pressure is expected to be higher for larger *sp* values, which is the case in the present model.

In summary, the HDM model predicts the temporal evolution of the impact force (pressure) during impact and considers the peak pressure for design, whereas the IACS method considers a single value at the end of an interaction, i.e., when the maximum contact area has been attained. The sensitivity study demonstrated that *wex* and $a_p$ are the most important parameters in the context of calculating ice pressures. For the IACS design scenario, no validation of *wex* is given, and experiments should be conducted to determine the best value for this constant and its influence on the designed ice pressures. Additionally, to clarify some of the concerns raised in this study, it is necessary to have detailed background information for the RMRS approach (RMRS, 2014) that explicitly links the ice class factors to physical parameters.

## *4 Conclusions and implications*

This paper discussed the methodology and underlying assumptions behind ice load formulations in the IACS and RMRS rules from a rigorously scientific perspective. The discussion was limited to ice crushing failure and deterministic solutions. In particular, Daley's ice load model and the Kurdyumov and Kheisin hydrodynamic model of ice crushing were used. The assumptions that underlie rule-based ice loads were placed in the context of current understanding of ice-structure interaction process, and the sensitivity of the results obtained using both methods to uncertainties in the input values was determined. A qualitative comparison between the two methodologies was presented. The main results are highlighted below.

- The advantage of the IACS approach is that it is relatively easy to understand. Moreover, a detailed derivation of the designed ice loads and a list of the underlying assumptions can be readily found in the literature.
- A complete understanding of the RMRS method and its assumptions remains challenging because the transition between the impact conditions, ice properties and class factors is neither straightforward nor clarified in the available scientific literature. Many important parameters, such as the ice geometry, ice mechanical characteristics, and vessel speed, are hidden in the class factors.
- The drawback of the ice load calculations with the Daley model and with the hydrodynamic model of ice crushing is that a few unsupported assumptions need be made. Each model includes three parameters that are not well known. In Daley's approach, these parameters are the ice pressure factor ($P_o$), the exponent in the Sanderson pressure-area relationship (*ex*), and the ice spalling parameter (*wex*), whereas in the hydrodynamic model, these parameters are the linear dependence between the crushed layer thickness and pressure ($n$ = 1.0), the characteristics of the ice strength $a_p$ (i.e., $k_p$ and $\mu$) and the ice spalling coefficient (*sp*).
- The assumed values of *wex* and $a_p$ are the most important assumptions. Unfortunately, these values are also the most uncertain. This result clearly indicates a knowledge gap that must be addressed in the future.

- Further studies with the hydrodynamic model are needed to elucidate whether it is possible to improve the model by including a different relationship between the pressure and the crushed layer thickness.

The information presented in this paper may help deepen our understanding of the scientific basis for rule-based ice loads. This improved understanding may be used for the development of calculation methodologies for scenarios that are not covered by the rule requirements (e.g., an ice floe hitting a floating or fixed structure, such as a drillship or floating production, storage and offloading unit).

## Acknowledgements

This work is a part of investigations conducted within the Centre for Autonomous Marine Operations and Systems (AMOS) and the Centre for Sustainable Arctic Marine and Coastal Technology (SAMCoT) at the Norwegian University of Science and Technology. The authors would like to acknowledge the support from the Research Council of Norway through the SAMCoT CRI (project no. 203471) and through the AMOS CoE (project no. 223254) and the support from all SAMCoT and AMOS partners.

## References

Appolonov, E.M., Didkovsky, A.V., Kuteinikov, M.A. and Nesterov, A.B., 2011. Improvement in design models for ice load evaluation under vessel impact against ice. Ships and Offshore Structures, Vol. 6, No. 3, pp. 249–256.

Appolonov, E.M., Didkovsky, A.V., Kuteinikov, M.A. and Nesterov, A.B., 2002. Совершенствование методологии определения ледовых нагрузок. Научно-технический сборник, Russian Maritime Register of Shipping, Issue 25, (in Russian).

Appolonov, E.M., 2003, Решение проблем обеспечения прочности судов ледового плавания и ледоколов в условиях круглогодичной эксплуатации в Арктике. PhD thesis, ЦНИИ им. акад. А.Н. Крылова, (in Russian).

Appolonov E.M., Evdoseev, A.N., Nesterov, A.B. and Timofeev, O.Y., 1996. О проекте новой редакции требований правил Российского Морского Регистра Судоходства к ледовым усилениям судов и ледоколов. Научно-технический сборник, Russian Maritime Register of Shipping, Issue 19, (in Russian).

Barents 2020, 2009. Assessment of international standards for safe exploration, production and transportation of oil and gas in the Barents Sea. Report No. 2009-1626, <www.dnv.no/Binaries/Barents_2020_report_%20phase_3_tcm155-519577.pdf>, (assessed 04.03.2015).

Budnevich, S.S. and Deryagin, B.V., 1952. Slipping of solid bodies on ice. Journal of Technical Physics, Vol. 22, Issue 12, (in Russian).

Daley, C., 1999. Energy based ice collision forces. In: Proceedings of the 15th International Conference on Port and Ocean Engineering under Arctic Conditions (POAC), Vol. 2, pp. 672–686.

Daley, C., 2000. Background notes to Design Ice Loads. IACS Ad-hoc group on Polar Class ships, Transport Canada.

Daley, C., 2004. A Study of the process-spatial link in ice pressure-area relationships, Prepared for National Research Council of Canada. PERD/CHC Report 7-108, pp. 1–24.

Daley, C., Kendrick, A. and Appolonov, E., 2001. Plating and framing design in the unified requirements for polar class ships. In: Proceedings of the 16th International Conference on Port and Ocean Engineering under Arctic Conditions, Vol. 2, pp. 779–791.

Daley, C., Tuhkuri, J. and Riska, K., 1998. The role of discrete failures in local ice loads. Cold Regions Science and Technology, Vol. 27, Issue 3, pp 197–211.

Dempsey, J.P., Palmer, A.C. and Sodhi, D.S., 2001. High pressure zone formation during compressive ice failure. Engineering Fracture Mechanics, Vol. 68, Issues 17–18, pp. 1961–1974.

Hong, L. and Amdahl, J., 2007. Plastic design of laterally patch loaded plates for ships. Marine Structures, Vol. 20, Issue 3, pp. 124–142.

IACS, 2011. Unified Requirements for Polar Ships: I2–Structural requirements for Polar Class ships, International Association of Classification Societies.

IMO, 2014. Considerations and adoption of amendments to mandatory instruments: Technical background to POLARIS. Maritime Safety Committee (Document MSC 94/3/7), International Maritime Organization.

Joensuu, A. and Riska, K., 1989. Jään ja raketeen välinen vuorovaikutus. Report M-88, Helsinki University of Technology, Otanemi, 57p., (in Finnish).

Jordaan, I.J., 2001. Mechanics of ice-structure interaction. Engineering Fracture Mechanics 68, pp.1923–1960.

Kalenchuk, S.V. and Kulesh, V.A., 2010. Ice strength of sea-going ship hulls: stages of development, problems, perspectives. Engineering School Bulletin Far Eastern Federal University, Electronic Scientific Journal, Vol. 3, No. 5, (in Russian).

Kim E. and Schulson, E.M., 2015. A phenomenological explanation of the pressure-area relationship for the indentation of ice: Two size effects in spherical indentation experiments. (Accepted for publication in Cold Regions Science and Technology on March,16).

Kurdyumov, V.A. and Kheisin, D.E., 1974. About definition of ice loads acting on icebreaker hull under impact. Proceedings of Leningrad Shipbuilding Institute, Issue 90, pp.95–100, (in Russian).

Kurdyumov, V.A. and Khesin, D. E., 1976. Hydrodynamic model of the impact of a solid ice. Pricladnaya Mechanica 12(10), pp. 103–109, (in Russian).

Kurdyumov, V.A., Tryaskin, V.N. and Kheisin, D.E., 1980. Определение ледовой прочности корпусов транспортных судов. Научно-технический сборник, Регистр СССР Вып.9: Теоретические и практические вопросы прочности и конструкции морских судов, 42–48, (in Russian).

Kurdyumov, V.A. and Kheisin D.E., 1984. Определение нагрузок при ударе судна вертикальным бортом о кромку ледяного поля, Научно-технический сборник, Регистр СССР Вып.14: Прочности и мореходные качества морских судов. Судовые энергетические установки, 3–10, (in Russian).

Likhomanov, V., Stepanov, I., Frederking, R. and Timco, G.W., 1998. Comparison of results of impact test on laboratory and natural freshwater ice with hydrodynamic model predictions. In: Proceedings of the 8th International Offshore and Polar Engineering Conference, Vol. 2, pp. 452–459.

Palmer, A.C. and Sanderson, T.J.O., 1991. Fractal crushing of ice and brittle solids. Proceedings of Mathematical and Physical Sciences 433(1889), pp. 469–477.

Palmer, A.C., Dempsey, J.P. and Masterson, D.M., 2009. A revised ice pressure-area curve and a fracture mechanics explanation. Cold Regions Science and Technology 56, pp. 73–76.

Popov, Y., Fadeyev, O., Kheisin, D. and Yakovlev, A., 1967. Strength of ships sailing in ice. Sudostroenie Publishing House, Leningrad, 223p, (in Russian).

Ralph, F. and Jordaan, I., 2013. Probabilistic methodology for design of arctic ships. Proceedings of the ASME 32nd International Conference on Ocean, Offshore and Arctic Engineering. Paper No. OMAE2013–10533.

Riska, K. and Kämäräinen, J., 2011. A review of ice loading and the evolution of the Finnish-Swedish Ice Class Rules. Transactions – Society of Naval Architects and Marine Engineers. Vol. 119, pp. 265–298.

Riska, K., 2011. Design of ice breaking ships. <www.eolss.net/Sample-Chapters/C05/E6-178-45-00.pdf>, (assessed 27.01.2015)

RMRS, 2014. Rules for the Classification and Construction of Sea-going Ships, Russian Maritime Register of Shipping, Vol. 1, Saint-Petersburg.

Sanderson, T.J.O., 1988. Ice mechanics. Risks to offshore structures. Graham and Trotman, London, UK.

Schulson, E.M. and Duval, P., 2009. Creep and fracture of ice. Cambridge University Press. 401p.

Sodhi, D.S., 2001. Crushing failure during ice-structure interaction. Engineering Fracture Mechanics 68(17–18), pp. 1889–1921.

Timco, G.W. and Sudom, D., 2013. Revisiting the Sanderson pressure-area curve: Defining parameters that influence ice pressure. Cold Regions Science and Technology 95, pp. 53–66.

Tunik, A., 1987. Impact ice loads on offshore structures. In: Proceedings of the 9th International Conference on Port and Ocean Engineering under Arctic Conditions, Vol. 1, pp. 485–493.

*Appendix*

Analytical solutions for the case of a glancing impact on a bow are available in the literature (Daley, 1999; Kurdyumov and Kheisin, 1974 and 1984; Kurdyumov et al., 1980; Popov et al., 1967). This section presents a step-by-step solution for a ship bow hitting a large ice floe with a rounded ice edge.

*Ship-ice interaction model: governing equations*

Consider a ship that is moving at speed $V$ and impacting a stationary ice edge with in-plane radius $R$. The collision occurs at point '*O*' and results in a normal force $Q$ along the collision line $Oy$; see a side view in Figure A1. This problem was first treated by Popov et al. (1967) and was later re-examined (Kurdyumov and Kheisin, 1974; Kurdyumov et al., 1980). The coordinate system and notation used in Kurdyumov and Kheisin (1974) and Kurdyumov et al. (1980) are used here with minor changes.

The collision can be modeled as if point $O$ is a single mass $M$ that corresponds to the ship mass (displacement). Motion occurs only in a plane normal to the ship's side at the collision point. This collision model was first developed by Popov et al. (1967) and includes a transformation of $M$ and $V$ into a reduced mass along the line of the collision, i.e., $M_n = M/C_0$ (where $C_0$ is the reduction coefficient) and velocity $V_n = \mathrm{V}\cdot l$ (where $l$ is the direction cosine), which is a projection of the ship's speed in the direction of the outward normal to the surface of the hull at the collision point. The ship's side is assumed to be rigid; only deformations of the ice are considered. The kinetic energy of the ship (reduced toward the line of impact) is dissipated via crushing of the ice edge. For the ship-ice floe system, the equation of motion is as follows:

$$M_n u_{pn} \frac{du_{pn}}{d\zeta} + \int_A p dA = 0, \qquad \text{(A0)}$$

where the first term is the derivative of the ship's kinetic energy with respect to position ζ and the second term is the total contact force, which is defined as the integral of the contact pressure *p* distributed over the nominal contact area *A*. The force depends on the geometry of the ice floe and the ship's depth of penetration into the ice (ζ).

To determine the ice pressure, the model assumes that there is an intermediate layer of crushed ice between the ship's side and the solid (undamaged) ice. This intermediate layer has a finite thickness (*h*) and is treated as an incompressible viscous medium. Its behavior is described using the simplified Navier-Stokes equations:

$$\rho\left(\frac{\partial u_i}{\partial t} + u_j \frac{\partial u_i}{\partial x_j}\right) = -\frac{\partial p}{\partial x_i} + \mu \frac{\partial^2 u_i}{\partial x_j \partial x_j} + f_i, \qquad \text{(A1)}$$

where $\rho$ and $\mu$ are the density and dynamic viscosity of the medium, respectively, $t$ is time, $u_i$ represents the velocity components of the flow, $p$ is the pressure, and $f_i$ represents the components of the body forces. The flow is symmetric relative to axis *Oy* and is mainly directed along axis *Ox* because the thickness of the layer is small.

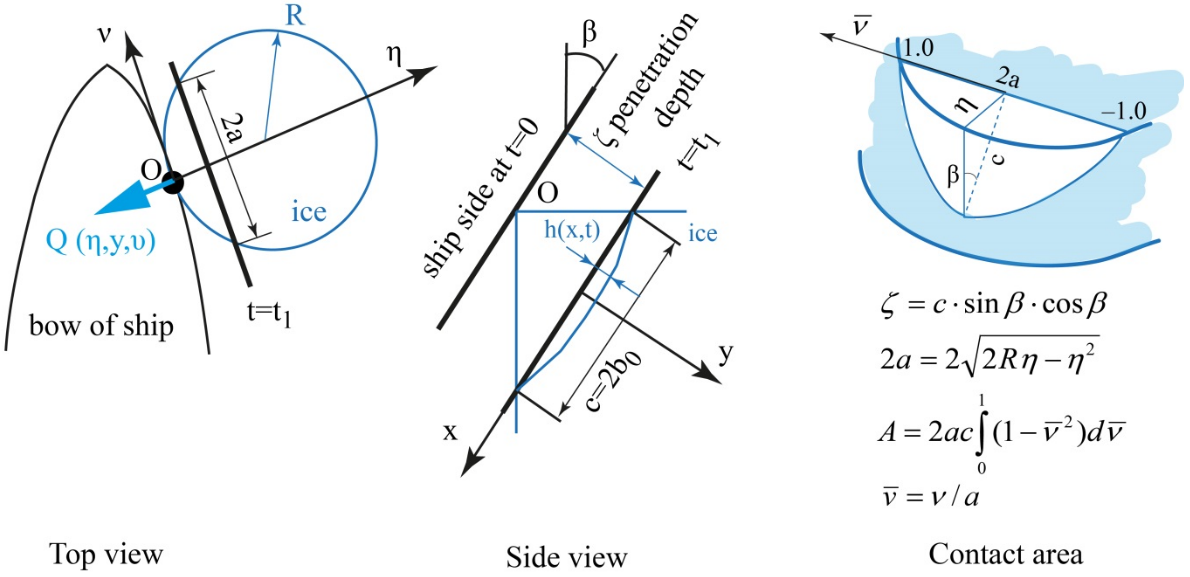


Figure A1. Contact geometry during an oblique collision with a rounded ice edge.

Equation A1 can be further simplified to the following:

$$\begin{cases} -\dfrac{\partial p}{\partial x} + \mu\left[\dfrac{\partial^2 u_x}{\partial y^2}\right] = 0 & \text{(A1a)} \\ \dfrac{\partial p}{\partial y} = 0 & \text{(A1b)} \end{cases}$$

Equations A1a and A1b are valid if the following assumptions are made:

1.1 The body forces with components $f_i$ are neglected.

1.2 The flow is parallel to the walls:

$$u_y = 0.$$

1.3 The variation of the pressure across the layer thickness is negligibly small:

$$\frac{\partial p}{\partial y} = 0 .$$

1.4 There is no flow in the *v* direction:

$$u_v = 0 .$$

1.5 The flow is fully developed, i.e., there is no change in the profile in the stream-wise direction:

$$\frac{\partial}{\partial t} = 0, \frac{\partial}{\partial x} = 0 .$$

1.6 The intermediate-layer is an incompressible and homogeneous media, which implies that

$$\frac{D\rho}{Dt} = -\rho \frac{\partial u_j}{\partial x_j} = 0, \frac{\partial u_x}{\partial x} + \frac{\partial u_y}{\partial y} = 0 . \qquad \text{(A1c)}$$

Ice failure is associated with the formation of two discontinuity surfaces, a *penetration surface* and a *fracture surface*. The penetration surface is defined by $y = 0$ and is the surface along the ship's side that moves at speed $u_y = u_{pn}$ and penetrates the ice ($u_{pn}$ is the penetration speed). The fracture surface is defined by $y = h(x)$ and is the surface along one side at which the ice is still an elastic body. A lubricating water layer is considered at $y = 0$ with a friction coefficient of 0.03–0.06 (Budnevich and Deryagin, 1952 via Popov et al. 1967). Shear stresses at this boundary are disregarded; the boundary conditions for Equations A1a and A1b are

1.7 $\tau(y=0)=\mu\frac{\partial u_x}{\partial y}=0$ and $u_y(y=0)=u_{pn}$ and

1.8 $u_x(y=h(x))=0, u_y(y=h(x))=0$.

Equations A1a – A1c contain no parameters that characterize the mechanical properties of solid ice; instead, only a single parameter, the dynamic viscosity of the crushed ice in the intermediate layer ($\mu$), is used. When solving Equations A1a – A1c, the following pressure distribution $p(x, t)$ over the thickness of the intermediate layer $h(x, t)$ is assumed:

$$p(x,t)=k_p\cdot h(x,t)^n, \tag{A2}$$

where $k_p$ and $n$ are empirical coefficients. This assumption introduces two parameters that characterize the crushed ice (i.e., $k_p$ and $n$). A linear relationship between $p$ and $h$ (i.e., $n = 1$) is assumed in Kurdyumov and Kheisin (1974, 1976), Kurdyumov et al. (1980) and RMRS.

Solving Equations A1a – A1c with the assumption defined by Equation A2 yields a basic relationship that relates the principal variables (i.e., the instantaneous pressure $p$ on the indenter's surface at a point with coordinate $x$ and instantaneous ship speed $u_{pn}$) and three ice parameters (i.e., $\mu$, $k_p$ and $n$):

$$p=\left(\frac{3}{2}\frac{n+3}{n}\mu u_{pn}\left(k_p\right)^{\frac{3}{n}}(b_0^2-x^2)\right)^{\frac{n}{n+3}}, \tag{A3}$$

where $b_0$ is the half-height of the hull-ice contact zone (see a side view in Figure A1).

<u>*Detailed derivation of A3*</u>

We begin with determining $u_x$ from Equation A1a:

$$-\frac{\partial p}{\partial x}+\mu\left[\frac{\partial^2 u_x}{\partial y^2}\right]=0,\Rightarrow \partial\frac{\partial u_x}{\partial y}=\frac{1}{\mu}\partial y\frac{\partial p}{\partial x},\Rightarrow \frac{\partial u_x}{\partial y}=\frac{1}{\mu}y\frac{\partial p}{\partial x}+C_1,\Rightarrow u_x=\frac{1}{2\mu}y^2\frac{\partial p}{\partial x}+C_1 y+C_2$$

The constants of integration can be determined from the boundary conditions (Pt. 1.7 and Pt. 1.8):

$$C_1=0, \qquad and \qquad C_2=-\frac{1}{2\mu}h^2\frac{\partial p}{\partial x}.$$

The velocity profile is

$$u_x=\frac{1}{2\mu}\frac{\partial p}{\partial x}(y^2-h^2).$$

Next, from Equation A1c we find $u_y$:

$$\frac{\partial u_y}{\partial y}=-\frac{\partial}{\partial x}\left(\frac{1}{2\mu}\frac{\partial p}{\partial x}(y^2-h^2)\right)=-\frac{1}{2\mu}\frac{\partial^2 p}{\partial x^2}y^2+\frac{\partial}{\partial x}\left(\frac{1}{2\mu}\frac{\partial p}{\partial x}h^2\right)$$

$$\frac{\partial u_y}{\partial y}=-\frac{1}{2\mu}\frac{\partial^2 p}{\partial x^2}y^2+\frac{1}{2\mu}\frac{\partial^2 p}{\partial x^2}h^2+\frac{1}{2\mu}\frac{\partial p}{\partial x}2h\frac{\partial h}{\partial x}$$

$$u_y=-\frac{1}{3}\frac{1}{2\mu}\frac{\partial^2 p}{\partial x^2}y^3+\frac{1}{2\mu}\frac{\partial^2 p}{\partial x^2}h^2 y+\frac{1}{2\mu}\frac{\partial p}{\partial x}2h\frac{\partial h}{\partial x}y+B_1$$

The constant of integration $B_1$ can be determined from the boundary conditions (Pt. 1.8):

$$u_y(y=h) = -\frac{1}{3}\frac{1}{2\mu}\frac{\partial^2 p}{\partial x^2}h^3 + \frac{1}{2\mu}\frac{\partial^2 p}{\partial x^2}h^3 + \frac{1}{2\mu}\frac{\partial p}{\partial x}2h^2\frac{\partial h}{\partial x} + B_1 = 0$$

$$B_1 = -\frac{1}{3}\frac{1}{\mu}\frac{\partial^2 p}{\partial x^2}h^3 - \frac{1}{2\mu}\frac{\partial p}{\partial x}2h^2\frac{\partial h}{\partial x}$$

The velocity profile along y-direction is

$$u_y = -\frac{1}{3}\frac{1}{2\mu}\frac{\partial^2 p}{\partial x^2}y^3 + \frac{1}{2\mu}\frac{\partial^2 p}{\partial x^2}h^2 y + \frac{1}{2\mu}\frac{\partial p}{\partial x}2h\frac{\partial h}{\partial x}y - \frac{1}{3}\frac{1}{\mu}\frac{\partial^2 p}{\partial x^2}h^3 - \frac{1}{2\mu}\frac{\partial p}{\partial x}2h^2\frac{\partial h}{\partial x}$$

Taking into account Pt. 1.7 (i.e., $u_y(y=0) = u_{pn}$) yields a differential equation that relates the pressure ($p$) and the crushed layer thickness ($h$):

$$h^3\frac{\partial^2 p}{\partial x^2} + 3\frac{\partial p}{\partial x}h^2\frac{\partial h}{\partial x} = -3\mu \cdot u_{pn}\,. \qquad \text{(A4)}^{(a)}$$

Substituting Equation A2 into Equation A4 results in the following:

$$p^{\frac{3}{n}}\frac{\partial^2 p}{\partial x^2} + \frac{3}{n}p^{\frac{3}{n}-1}\left(\frac{\partial p}{\partial x}\right)^2 = -3\mu \cdot \left(k_p\right)^{\frac{3}{n}}u_{pn}\,. \qquad \text{(A5)}$$

Equation A5 can be rearranged to yield the following:

$$\frac{\partial\left(\frac{\partial p}{\partial x}p^{\frac{3}{n}}\right)}{\partial x} = -3\mu \cdot \left(k_p\right)^{\frac{3}{n}}u_{pn}$$

[(a)]Alternatively, Equation A4 can be derived first – by determining $u_x$ from (Equation A1a); next – by introducing the expressions of the horizontal flux $flux(x,t) = \int_0^{h(x,t)} u_x(t)dy = -\frac{1}{3\mu}\frac{\partial p}{\partial x}h^3$ and the mass conservation: $\frac{\partial h}{\partial t} + \frac{\partial flux}{\partial x} = 0, \frac{\partial h}{\partial t} = u_{pn}$ ; and then – by substituting the flux equation into the equation of mass conservation.

Using substitution, the following equation is obtained:

$$p = \xi^{\frac{n}{n+3}}, \frac{\partial p}{\partial x} = \frac{n}{n+3} \xi^{-\frac{3}{n+3}} \frac{\partial \xi}{\partial x}.$$

Equation A5 becomes

$$\frac{\partial \left( \frac{n}{n+3} \xi^{-\frac{3}{n+3}} \frac{\partial \xi}{\partial x} \xi^{\frac{3n}{n(n+3)}} \right)}{\partial x} = -3\mu \cdot \left(k_p\right)^{\frac{3}{n}} u_{pn},$$

$$\frac{\partial^2 \xi}{\partial x^2} = -3\mu \cdot \left(k_p\right)^{\frac{3}{n}} u_{pn} \frac{n+3}{n}, \text{ and}$$

$$\frac{\partial \xi}{\partial x} = -3\mu \cdot \left(k_p\right)^{\frac{3}{n}} u_{pn} \frac{n+3}{n} x + C_1, \Rightarrow \xi = -\frac{3}{2} \mu \cdot \left(k_p\right)^{\frac{3}{n}} u_{pn} \frac{n+3}{n} x^2 + C_1 x + C_2.$$

Determine $C_1$ and $C_2$ by accounting for the lack of a pressure gradient at $x = 0$ and $p = 0$ at $x = b_0$:

$$C_1 = 0, C_2 = \frac{3}{2} \mu \cdot \left(k_p\right)^{\frac{3}{n}} u_{pn} \frac{n+3}{n} b_0^{\,2}.$$

Hence,

$$\xi = -\frac{3}{2}\mu \cdot (k_p)^{\frac{3}{n}} u_{pn} \frac{n+3}{n} x^2 + \frac{3}{2}\mu \cdot (k_p)^{\frac{3}{n}} u_{pn} \frac{n+3}{n} b_o{}^2 = \frac{3}{2}\mu \cdot (k_p)^{\frac{3}{n}} u_{pn} \frac{n+3}{n} (b_0^2 - x^2)$$

$$p = \left( \frac{3}{2}\frac{n+3}{n} \mu u_{pn} (k_p)^{\frac{3}{n}} (b_0^2 - x^2) \right)^{\frac{n}{n+3}} \; or \; p = \left( \frac{3}{2}\frac{n+3}{n} \mu u_{pn} (k_p)^{\frac{3}{n}} (sp^2 - \bar{x}^2) \left( \frac{b_0}{sp} \right)^2 \right)^{\frac{n}{n+3}} .$$

Here, the following transformations are introduced:

$$\bar{x} = \frac{x}{b_{eff}}, sp = \frac{b_0}{b_{eff}}, \tag{A6}$$

where $\bar{x}$ is a dimensionless coordinate and *sp* is the ice spalling parameter that accounts for the reduction in the height of the hull-ice contact area.

The final expressions for the ice impact load parameters, such as the impact force, pressure, depth of penetration, maximum load height, and their histories are determined by solving Equation A0. $u_{pn}$ is found by substituting Equations A3 and A6 into Equation A0. The substitution yields

$$M_n u_{pn} \frac{du_{pn}}{d\zeta} + u_{pn}^{\frac{n}{n+3}} \left( \frac{3}{2}\frac{n+3}{n} \mu (k_p)^{\frac{3}{n}} \right)^{\frac{n}{n+3}} J_1 \int_{2a} c^{\frac{3n+3}{n+3}} da = 0 . \tag{A7}$$

Here, *c* and *a* represent the dimensions of the nominal contact area (Figure A1) and

$$J_1 = 2^{-\frac{2n}{n+3}} \cdot sp^{-\frac{3n+3}{n+3}} \cdot \int_0^1 \left( sp^2 - \bar{x}^2 \right)^{\frac{n}{n+3}} d\bar{x} .$$

When small penetrations are considered ($\eta_{max} << R$), $c$ and $a$ can be approximated as

$$a \approx \sqrt{\frac{2R\zeta}{\cos\beta}}, c \approx \frac{\zeta(1-\bar{v}^2)}{\sin\beta\cos\beta}.$$

The expression for $c$ accounts for the deviation of the contact shape from a rectangle toward a parabolic segment, where $\bar{v} = \frac{v}{a}$, $\bar{v} \in [-1;1]$ is the normalized out-of-plane coordinate (see Figure A1). Substituting the expressions for $a$ and $c$ into Equation A7 and using $\zeta = 0$, $u_{pn} = V_n$ and $\int_A p dA = 0$, the following relationships can be obtained:

$$u_{pn} = \left\{ V_n^{\frac{n+6}{n+3}} - \frac{n+6}{n+3}\frac{1}{M_n}\left(\frac{3}{2}\frac{n+3}{n}\mu(k_p)^{\frac{3}{n}}\right)^{\frac{n}{n+3}} J_1 \int_0^{\zeta}\int_{2a} c^{\frac{3n+3}{n+3}} da d\zeta \right\}^{\frac{n+3}{n+6}}$$

or

$$u_{pn} = \left\{ V_n^{\frac{n+6}{n+3}} - \left(\frac{n+6}{n+3}\right)\left(\frac{2n+6}{9n+15}\right)\frac{\left(\frac{3}{2}\frac{n+3}{n}\mu(k_p)^{\frac{3}{n}}\right)^{\frac{n}{n+3}}}{M_n \cos^{\frac{7n+9}{2n+6}}\beta \cdot \sin^{\frac{3n+3}{n+3}}\beta} J_1 J_2 \zeta^{\frac{9n+15}{2n+6}} \right\}^{\frac{n+3}{n+6}}. \quad \text{(A8)}$$

Here, $J_1$ and $J_2$ are numerical factors that account for ice edge spalling effects and deviations of the contact shape from a rectangle:

$$J_2 = 2\int_0^1 \left(1-\overline{v}^2\right)^{\frac{3n+3}{n+3}} d\overline{v} \, .$$

Equations A3 and A8 represent a generalization of the results of Kurdyumov and Kheisin (1974). If $n = 1$, Equations A3 and A8 are the same as those of Kurdyumov and Kheisin (1974), i.e.,

$$p = \sqrt[4]{6\mu u_{pn} k_p^3 (sp^2 - \overline{x}^2)\left(\frac{b_0}{sp}\right)^2} \, , \tag{A9}$$

where

$$u_{pn} = \left\{ V_n^{\frac{7}{4}} - \frac{7}{12M_n} \frac{\left(6\mu k_p{}^3\right)^{\frac{1}{4}} \sqrt{2R}}{\cos^2\beta \sin^{\frac{3}{2}}\beta} J_1 J_2 \zeta^3 \right\}^{\frac{4}{7}} \text{ and}$$

$$J_1 = (2sp^3)^{-\frac{1}{2}} \int_0^1 \left(sp^2 - \overline{x}^2\right)^{\frac{1}{4}} d\overline{x} \text{ and } J_2 = 2\int_0^1 (1-\overline{v}^2)^{\frac{3}{2}} d\overline{v} \, . \tag{A10}$$

*Final expressions for the ice impact load parameters*

The final expressions for the ice impact load parameters are presented below for the case in which $n = 1$. The *line load* ($q$) is given by

$$q = \int_{2b_{eff}} p dx = 2\alpha^{-\frac{3}{2}} \left(6\mu u_{pn} k_p^3\right)^{\frac{1}{4}} \left(b_0\right)^{\frac{3}{2}} \int_0^1 \left(sp^2 - \bar{x}^2\right)^{\frac{1}{4}} d\bar{x} . \tag{A11}$$

The *total contact force* is given by

$$Q = \int_A p dA = \left(6\mu u_{pn} k_p^3\right)^{\frac{1}{4}} J_1 J_2 \frac{\sqrt{2R}}{\cos^2(\beta)\sin^{\frac{3}{2}}(\beta)} \zeta^2 . \tag{A12}$$

At a certain penetration depth, the maximum pressure, which is the pressure at the center of the load patch ( $\bar{v} = \bar{x} = 0$ ), has a peak ($p_{peak}$). The solution for $p_{peak}$ is given by

$$\frac{\partial p}{\partial \zeta} = 0 .$$

Hence,

$$p_{peak} = \underbrace{\frac{1}{\sqrt{2}}\left(\frac{12}{13}\right)^{\frac{1}{6}}\left(\frac{6}{13}\right)^{\frac{1}{7}}\left(\frac{1}{J_1 J_2}\right)^{\frac{1}{6}}\left(\frac{sp^2 - \bar{x}^2}{sp^2}\right)^{\frac{1}{4}}}_{\text{Has a value of 0.662 for } sp\text{=1.06}} (1-\bar{v}^2)^{\frac{1}{2}} \overbrace{\left(6\mu k_p^3\right)^{\frac{5}{24}} (2R)^{-\frac{1}{12}}}^{\text{Ice characteristics}} \underbrace{(V_n)^{\frac{13}{24}} (M_n)^{\frac{1}{6}} \cos^{-\frac{1}{6}}(\beta) \sin^{-\frac{1}{4}}(\beta)}_{\text{Impact conditions}} .$$

The solution for the *maximum line load* is given by

$$\frac{\partial q}{\partial \zeta} = 0 .$$

Hence,

$$q_{\max} = \frac{1}{\sqrt{2^3}}\left(\frac{12}{7}\right)^{\frac{1}{2}}\left(\frac{7}{9}\right)^{\frac{1}{2}}\left(\frac{2}{9}\right)^{\frac{1}{7}}\left(\frac{1}{J_1J_2}\right)^{\frac{1}{2}} 2(\alpha)^{-\frac{3}{2}}\int_0^1\left(\alpha^2-\bar{x}^2\right)^{\frac{1}{4}}d\bar{x}\left(6\mu k_p^3\right)^{\frac{1}{8}}(2R)^{-\frac{1}{4}}(V_n)^{\frac{9}{8}}(M_n)^{\frac{1}{2}}\cos^{-\frac{1}{2}}(\beta)\sin^{-\frac{3}{4}}(\beta).$$

The solution for the *maximum contact force* is given by

$$\frac{\partial Q}{\partial \zeta} = 0 \text{ and}$$

$$Q_{\max} = \left(\frac{12}{7}\right)^{\frac{2}{3}}\left(\frac{3}{17}\right)^{\frac{1}{7}}\left(\frac{14}{17}\right)^{\frac{2}{3}}(J_1J_2)^{\frac{1}{3}}\left(6\mu k_p^3\right)^{\frac{1}{12}}(2R)^{\frac{1}{6}}(V_n)^{\frac{17}{12}}(M_n)^{\frac{2}{3}}\cos^{-\frac{2}{3}}(\beta)\sin^{-\frac{1}{2}}(\beta).$$

The *maximum penetration* depth is determined from Equation A10 by setting $u_{pn} = 0$. The solution becomes

$$\zeta_{\max} = \left(\frac{12}{7}\right)^{\frac{1}{3}}\left(\frac{1}{J_1J_2}\right)^{\frac{1}{3}}\left(6\mu k_p^3\right)^{-\frac{1}{12}}(2R)^{-\frac{1}{6}}(V_n)^{\frac{7}{12}}(M_n)^{\frac{1}{3}}\cos^{\frac{2}{3}}(\beta)\sin^{\frac{1}{2}}(\beta).$$

Using the transformation

$$u_{pn} = V_n\left(1-\bar{\zeta}^3\right)^{\frac{4}{7}}, \tag{A13}$$

where $\bar{\zeta} = \dfrac{\zeta}{\zeta_{\max}}$ is the relative penetration depth, Equations A9, A11 and A12 can be rewritten as

$$p = 1.238 p_{peak} \left(1 - \bar{\zeta}^{3}\right)^{\frac{1}{7}} \bar{\zeta}^{\frac{1}{2}}, \tag{A14}$$

$$q = 1.406 q_{\max} \left(1 - \bar{\zeta}^{3}\right)^{\frac{1}{7}} \bar{\zeta}^{\frac{3}{2}} \text{ and} \tag{A15}$$

$$Q = 1.238 Q_{\max} \left(1 - \bar{\zeta}^{3}\right)^{\frac{1}{7}} \bar{\zeta}^{2}. \tag{A16}$$

Equations A14 – A16 are valid if the load that is required to break the ice by bending, $Q_b$, (or buckling, $Q_e$) exceeds $Q_{\max}$. If $\min\{Q_b, Q_e\} \leq Q_{\max}$, then ice failure begins before the maximum penetration is reached; hence, the ship will maintain a certain speed, $u_{pn}/V_n = k$. By reworking Equations A14 – A16 in terms of the parameter $k$, the following relationships are obtained:

$$\frac{\zeta}{\zeta_{\max}} = \left(1 - k^{\frac{7}{4}}\right)^{\frac{1}{3}}; \ \zeta = \zeta_{\max} f_{\zeta}, \tag{A17}$$

$$\frac{p}{p_{peak}} = 1.24 \left(1 - k^{\frac{7}{4}}\right)^{\frac{1}{6}} k^{\frac{1}{4}}; \ p = p_{peak} f_{p}, \tag{A18}$$

$$\frac{q}{q_{\max}} = 1.41 \left(1 - k^{\frac{7}{4}}\right)^{\frac{1}{2}} k^{\frac{1}{4}}; \ q = q_{\max} f_{q} \text{ and} \tag{A19}$$

$$\frac{Q}{Q_{\max}} = 1.46\left(1 - k^{\frac{7}{4}}\right)^{\frac{2}{3}} k^{\frac{1}{4}};\ Q = Q_{\max} f_Q\,. \tag{A20}$$

For practical applications of these expressions, the following compact form, in which $sp$ = 1.06, is often used to estimate the ice loads on ship structures:

$$p = 0.662(V\ )^{\frac{13}{24}}(M)^{\frac{1}{6}} a_p (2R)^{-\frac{1}{12}} F_p\left(\frac{x}{L}\right) f_p\,, \tag{A21}$$

$$q = 0.665(V\ )^{\frac{9}{8}}(M)^{\frac{1}{2}}(a_p)^{\frac{3}{5}}(2R)^{-\frac{1}{4}} F_q\left(\frac{x}{L}\right) f_q\,, \text{ and} \tag{A22}$$

$$Q\ = 0.875(V)^{\frac{17}{12}}(M)^{\frac{2}{3}}(a_p)^{\frac{2}{5}}(2R)^{\frac{1}{6}} F_Q\left(\frac{x}{L}\right) f_Q\,. \tag{A23}$$

The maximum height of the hull-ice contact is

$$b\ = \frac{\zeta}{\cos(\beta)\sin(\beta)} = 1.344(V)^{\frac{7}{12}}(M)^{\frac{1}{3}}(a_p)^{-\frac{2}{5}}(2R)^{-\frac{1}{6}} F_b\left(\frac{x}{L}\right) f_b\,. \tag{A24}$$

Here, the impact location is represented by $x/L$ (where $x$ is the distance from the forward perpendicular to the collision point and $L$ is the ship length), and the following parameters are introduced:

$$a_p = \left(6\mu k^3\right)^{\frac{5}{24}};$$

$$F_p = l^{\frac{13}{24}}\left(C_o\right)^{-\frac{1}{6}}\cos^{-\frac{1}{6}}(\beta)\sin^{-\frac{1}{4}}(\beta);$$

$$f_p = 1.24\left(1-k^{\frac{7}{4}}\right)^{\frac{1}{6}}k^{\frac{1}{4}}$$

$$F_q = l^{\frac{9}{8}}\left(C_o\right)^{-\frac{1}{2}}\cos^{-\frac{1}{2}}(\beta)\sin^{-\frac{3}{4}}(\beta);$$

$$f_q = 1.41\left(1-k^{\frac{7}{4}}\right)^{\frac{1}{2}}k^{\frac{1}{4}}$$

$$F_Q = l^{\frac{17}{12}}\left(C_o\right)^{-\frac{2}{3}}\cos^{-\frac{2}{3}}(\beta)\sin^{-\frac{1}{2}}(\beta);$$

$$f_Q = 1.46\left(1-k^{\frac{7}{4}}\right)^{\frac{2}{3}}k^{\frac{1}{4}}$$

$$F_b = l^{\frac{7}{12}}\left(C_o\right)^{-\frac{1}{3}}\cos^{-\frac{1}{3}}(\beta)\sin^{-\frac{1}{2}}(\beta);$$

$$f_b = \left(1-k^{\frac{7}{4}}\right)^{\frac{1}{3}}$$

Here, $a_p$ is the ice strength factor, $l$ is the direction cosine, $C_o$ is the mass reduction coefficient defined according to Popov et al. (1967) or Daley (2000), $\beta$ is the frame angle, $R$ is the radius of the ice edge, $V$ is the forward velocity at the moment of impact, $M$ is the mass of the vessel (displacement), and $f_p$ ($f_p \leq 1.0$) is a coefficient that accounts for the bending and buckling failure of ice. When $f_p = 1.0$, only ice crushing is considered.